Thin Films with Densely, Regularly Packed Nanochannels: Preparation, Characterization, and Applications

Guojun Liu* and Jianfu Ding

Department of Chemistry, University of Calgary, 2500 University Drive, NW, Calgary, Alberta, Canada, T2N 1N4

T. Hashimoto and K. Kimishima

Department of Polymer Chemistry, Kyoto University, Kyoto 606-8501, Japan

F. M. Winnik and S. Nigam

Brockhouse Institute for Materials Research, Department of Chemistry, McMaster University, 1280 Main Street West, Hamilton, Ontario, Canada L8S 4M1

Received April 2, 1999. Revised Manuscript Received June 8, 1999

A poly(*tert*-butyl acrylate)-*block*-poly(2-cinnamoylethyl methacrylate), P*t*BA-*b*-PCEMA, sample was synthesized and characterized. After annealing at 105 ± 2 °C, the P*t*BA block formed densely packed cylinders inside the PCEMA matrix. Thin films of the diblock were obtained by microtomy. After PCEMA photo-cross-linking, the *tert*-butyl groups of P*t*BA were hydrolyzed, leaving poly(acrylic acid) chains in the loosely packed nanometer-sized cylinders. The permeability of water across such films varied by several orders of magnitude, depending on the pH of the aqueous medium or the types of cations in it. The possibility of using such nanochannels as templates for making further nanostructures was tested by filling the nanochannels with CdS or Fe_2O_3 nanoparticles.

I. Introduction

Thin films with uniformly sized nanochannels packed at high density and regularity have many potential applications. The films can, for example, serve as size-specific membranes,[1] and the channels can serve as template for metallic, semiconductor, or magnetic inorganic nanostructure preparation.[2,3] Reported in this paper are the preparation and characterization of such thin films from a diblock copolymer. Also will be reported are the unique water permeation properties of such nanochannels and the preparation of CdS and iron oxide in such nanochannels.

As communicated previously,[4,5] such thin films are prepared from poly(*tert*-butyl acrylate)-*block*-poly(2-cinnamoylethyl methacrylate) or P*t*BA-*b*-PCEMA. They are prepared by taking advantage of the self-assembling properties of the diblock in bulk, the photo-cross-linkability of PCEMA, and the easy hydrolyzability of the *tert*-butyl groups of the P*t*BA block. The two blocks of a diblock copolymer, $(A)_n(B)_m$, segregate from one another in bulk due to their incompatibility.[6,7] The

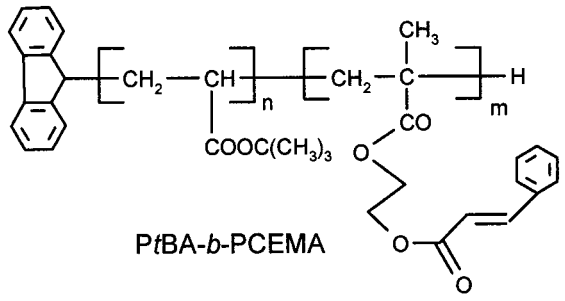

P*t*BA-*b*-PCEMA

smallest dimension (radius for cylinders and thickness for lamellae) of a segregated A or B domain is similar to that of the individual A or B coils in a good solvent. The shape of the A or B domain varies with the relative *n* and *m* values and the temperature. As the volume fraction of B increases gradually to ∼50%, the shape of the B domain normally changes from spheres (∼17%) to cylinders (∼28%), to gyroids (∼38%), and finally to lamella (∼50%). Domains with different shapes are formed to minimize the system's free energy. For preparing thin films with nanochannels, a P*t*BA-*b*-PCEMA sample with 3.8×10^2 *t*BA and 6.4×10^2 CEMA units or a P*t*BA volume fraction of 0.26 is used.[8] In annealed solid of such a diblock, the P*t*BA block forms

(1) Matsuura, T. *Synthetic Membranes and Membrane Separation Process*; CRC Press: Boca Ranton, 1993.
(2) Ozin, G. A.; Chomski, E.; Khushalani, D.; McClachlan, M. J. *Curr. Opin. Colloid Interface Sci.* **1998**, *3*, 181 and references therein.
(3) Martin, C. R. *Science* **1994**, *266*, 1961 and references therein.
(4) Liu, G.; Ding, J.; Guo, A.; Herfort, M.; Bazett-Jones, D. *Macromolecules* **1997**, *30*, 1851.
(5) Ding, J.; Liu, G. *Adv. Mater.* **1998**, *10*, 69.
(6) Bates, F. S.; Fredrickson, G. H. *Annu. Rev. Phys. Chem.* **1990**, *41*, 525.
(7) Hesagawa, H.; Hashimoto, T. In *Comprehensive Polymer Science*; Pergamon Press: London, 1996.
(8) The P*t*BA block in this sample has a volume fraction of 26%, as calculated from $n/m = 0.59$ and from the densities of PCEMA and P*t*BA, 1.25 and 1.02 g/mL, respectively.

10.1021/cm990184k CCC: $18.00
Published on Web 07/17/1999

Scheme 1. Schematic Illustration of the Processes Involved in the Preparation of Thin Films with Nanochannels from P*t*BA-*b*-PCEMA[a]

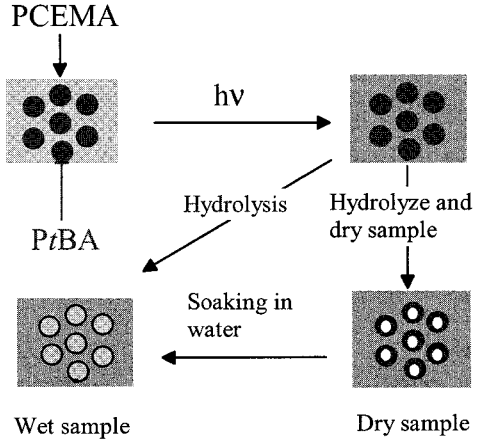

approximately hexagonally packed cylinders dispersed in the PCEMA matrix. Films, 0.05−2.0 μm thick, are obtained by microtomy. The PCEMA matrix is then photo-cross-linked and the *tert*-butyl groups are removed from the cylindrical domains yielding nanochannels partially filled with poly(acrylic acid), PAA, chains as illustrated schematically in Scheme 1.

The methodology used here for thin-film preparation is similar to that used by Lee et al.[9] In their case, poly[(4-vinylphenyl)dimethyl-(2-oxopropyl)silane]-*block*-polyisoprene, PVPDMPS-*b*-PI, was used. Bulk films, ∼20 μm thick, were exposed to acid to cross-link the PVPDMPS matrix. Void channels were produced by degrading PI cylinder from ozonolysis. No gas or liquid permeability was, however, found for these films probably due to poor block segregation in the samples. After the report of Liu et al.,[4] Park et al.[10] reported the formation of periodic arrays of holes in polystyrene-*block*-polybutadiene films by degrading spherical domains of polybutadiene for lithographic applications. Hashimoto et al.[11] reported the preparation of thin films with void channels from polystyrene-*block*-polyisoprene by degrading PI gyroids inside a PS matrix. Nickel metal could then be plated inside the channels. Organic polymeric membranes with narrow pore size distributions can also be prepared from the track-etch method.[12,13] The cylindrical pores generated from this method are, however, not regularly packed and their packing density is about 2 orders of magnitude lower than those obtained from the method reported in this paper. More recently, nanopores with regular packing were produced in polymer films by the nanoimprinting method.[14] The potential of the nanoimprinting method in preparing films with large surface areas, however, remains to be demonstrated.

(9) Lee, J.-S.; Hirao, A.; Nakahama, S. *Macromolecules* **1989**, *22*, 2602.
(10) Park, M.; Harrison, C.; Chaikin, P. M.; Register, R. A.; Adamson, D. H. *Science* **1997**, *276*, 1401.
(11) Hashimoto, T.; Tsutsumi, K.; Funaki, Y. *Langmuir* **1997**, *13*, 6869.
(12) Fleischer, R. L.; Price, P. B.; Walker, R. M. *Nuclear Tracks in Solids*; University of California Press: Berkeley, 1975.
(13) Yoshida, M.; Asano, M.; Sagranj, A.; Omichi, H.; Spohr, R.; Vetter, J.; Katakai, R. *Macromolecules* **1996**, *29*, 8987.
(14) Chou, S. Y.; Krauss, P. A.; Restrom, P. J. *J. Vacuum Sci., Technol. B* **1996**, *14*, 4129.

Table 1. Molecular Characteristics of the Diblock Used

n/m from NMR	$\bar{M}_w/\bar{M}_n$ from GPC	$10^{-4}\bar{M}_w$ (g/mol) LS	$10^{-2}m$	$10^{-2}m$
0.59	1.18	22.1	3.8	6.4

II. Experimental Section

Polymer Synthesis and Characterization. The precursor to P*t*BA-*b*-PCEMA was P*t*BA-*b*-P(HEMA-TMS), where P(HEMA-TMS) denotes poly(2-trimethylsilylethyl methacrylate). P*t*BA-*b*-P(HEMA-TMS) was prepared by anionic polymerization as described previously.[4−5,15] The TMS group was removed by hydrolysis in methanol. Reacting poly(*tert*-butyl acrylate)-*block*-poly(2-hydroxylethyl methacrylate) with cinnamoyl chloride yielded PS-*b*-PCEMA. The sample was characterized by gel permeation chromatography (GPC), NMR, and light scattering (LS). From ratioing the intensities of ^{1}H peaks of P*t*BA to those of PCEMA the repeat unit ratio between PS and PCEMA, n/m, was determined to 0.59. The GPC polydispersity index, $\bar{M}_w/\bar{M}_n$, of 1.18 in terms of PS standards suggests a narrow molar mass distribution. Using n/m and the LS molar mass of 2.2×10^5 g/mol, we calculated the n and m values of 3.8×10^2 and 6.4×10^2 for the sample (Table 1).

Film Preparation and Water Permeability Test. P*t*BA-*b*-PCEMA films or disks, 1−4 mm thick, were prepared by evaporating a ∼20%, by volume, polymer solutions in toluene in polyethylene bottles or capsules over 3−4 days. The samples were then annealed at 60 ± 5 °C and 105 ± 2 °C for 3 days and 3 weeks, respectively.

Such a bulk sample with the size of $\sim 3 \times 3 \times 2$ mm^3 was embedded in an epoxy resin and cured at 60 °C overnight. The sample was then equilibrated for 24 h with toluene vapor in a sealed vial. The sorption of toluene softened the annealed P*t*BA-*b*-PCEMA sample and allowed the microtoming of films as thick as 2 μm. Films, 50 nm thick, used for morphological studies by TEM, were picked up by carbon-coated copper grids. For UV irradiation, films with thicknesses in the range of 0.050 and 2 μm were picked up and placed on a quartz plate. Upon drying, the films stuck to the quartz plate well probably due to surface tension effect. To obtain uniform cross-linking across the film thickness, the films were irradiated for an equal period of time on each side using light which had passed a 310-nm cutoff filter. The typical PCEMA double-bond conversion used was ∼40%.

To hydrolyze the *tert*-butyl groups, the cross-linked 2-μm-thick films, supported on gold grids, were soaked in a 0.050 M $(CH_3)_3SiI$ solution in CH_2Cl_2 for 2 weeks and then in a water/methanol (v/v = 5/95) mixture for 2 days. To hydrolyze the *tert*-butyl groups in 50-nm-thick films which were used for TEM studies, 2−3 days were allowed for the reaction between the films and $(CH_3)_3SiI$.

For testing water permeation across the nanochannels, a 2-μm-thick PS-*b*-PAA film was sandwiched between two polyethylene films (30 μm thick) with paraffin linings (∼10 μm thick), where both the polyethylene films and linings had a 1-mm hole in the center. The softer paraffin linings were used to ensure sealing between polyethylene films and the membrane. After the membrane was sandwiched, the composite film was lightly pressed and mounted between two arms of a U-tube with a ground interface and a circular opening with a diameter of ∼1.5 mm. The two sides were held together by a clamp. Water flowed from one arm of a U-tube to the other due to height difference h in the water levels between the two arms.

For a quantitative analysis of the h variation data, we note that water transportation rate in terms of volume, V, lost in unit time on the higher water level side is[16]

(15) Henselwood, F., Liu, G. *Macromolecules* **1997**, *30*, 488.
(16) Hautojarvi, J.; Kontturi, K.; Nasman, J. H.; Svarfvar, B. L.; Viinikka, P.; Vuoristo, M. *Ind. Eng. Chem. Res.* **1996**, *35*, 450.

$$-\frac{dV}{dt} = PA\frac{p}{l} \quad (1)$$

where P is the permeability constant of the nanochannels, A is the total permeable nanochannel cross-section area, l is the thickness of the membrane, and p is the pressure drop across the two sides of the U-tube. If the cross-section area of the U-tube is σ,

$$-\frac{dV}{dt} = -\frac{\sigma\, dh}{2\, dt} \quad (2)$$

where $^1/_2$ accounts for the fact that h changes due to a water height decrease in one arm and an increase in the other. The p term in eq 1 is related to h by

$$p = \rho g h \quad (3)$$

with ρ the water density and g the gravitational acceleration constant. Inserting eqs 2 and 3 into eq 1 and performing integration yields

$$h = h_0 \exp(-\lambda t) \quad (4)$$

where

$$\lambda = \frac{2PA\rho g}{\sigma l} \quad (5)$$

Thus, h should decrease exponentially with time.

Small-Angle X-ray Scattering and TEM Studies. The small-angle X-ray scattering, SAXS, experiment was conducted using a ~1-mm-thick disk prepared as described above. The slit-collimated X-ray beam impinged upon the diblock disk along the direction normal to the disk plane. A one-dimensional position-sensitive proportional counter was used, 1895 mm away from the sample, to detect the scattered X-ray. Because the incident beam had a finite size, a procedure was used to desmear the measured SAXS profile.[17,18]

Slices with a thickness of ~50 nm were used for TEM studies. The sectioned samples were stained with OsO_4 vapor overnight before viewing under a Hitachi-7000 electron microscope (TEM) operated at 100 kV. For silicon-specific imaging, a Zeiss 902 microscope equipped with an energy loss spectrometer was used.

CdS and Fe_2O_3 Formation in the Nanochannels. Films, 2 μm thick, were placed in a solution of ferrous chloride, $FeCl_2 \cdot 4H_2O$ (0.250 g, 0.050 M) in water (25 mL). It was purged with nitrogen for 24 h at room temperature. The films were then removed from the solution and washed with water until the eluant was iron-free, as determined by the thiocyanate test.[19] The iron-loaded membrane was then immersed in an aqueous NaOH solution (20 mL, 1 M) and heated at 70 °C for 2 h under nitrogen. A constant flow of oxygen was then bubbled through the solution for 16 h at 70 °C. The solution was cooled to room temperature, whereupon the thin films were removed and washed thoroughly in a water/methanol (1/1 v/v) solution. The thin films, initially colorless, turned light brown. To increase the level of iron oxide incorporation in the membrane, the procedure was repeated two more times for each thin film. The membranes became progressively darker, but they kept their integrity throughout the treatment.

To introduce Cd^{2+}, 2-μm-thick films were soaked in a 0.10 M $Cd(Ac)_2$ solution of methanol/water (v/v = 50/50) for 30 h. The films were then taken out of the solution, rinsed briefly with water, and exposed for 2 h to H_2S generated from reacting a saturated $Na_2S \cdot 9H_2O$ aqueous solution with gradually added concentrated hydrochloric acid. This procedure was repeated two more times for each film and the films looked bright yellow after CdS loading.

The electron diffraction patterns of the CdS and Fe_2O_3 particles were obtained using the Hitachi instrument at an aperture of 3.5 μm^2. The instrument was calibrated using Au as a standard.

Polymer Density Measurement. A solution of PCEMA or P*t*BA in toluene at ~20% by mass was cast on a glass slide. The film was left drying at room temperature for 1 day and at 110 °C under vacuum for another day. The film was then cut into pieces of 9-mm^2-large and 1-mm-thick. The small pieces were placed in a 8-mL vial with 0.9909 g of $CaCl_2$. Water was gradually added into the vial with stirring. At the critical point when the polymer films were about to settle but still remained suspended, the water addition was stopped and the total amount of water added was determined. The density of the final aqueous solution at this stage at 20 °C was found from a handbook.[20] This value was assumed to be the density of the polymer. The densities determined for PCEMA and P*t*BA were 1.25 and 1.02 g/cm^3, respectively. The density value of 1.02 g/cm^3 for P*t*BA was in good agreement with the literature value of 1.00 g/cm^3.[21]

III. Results and Discussion

Synthesis of Films with Ordered Nanochannels. All the films described here were obtained from a P*t*BA-*b*-PCEMA copolymer consisting of 3.8×10^2 *t*BA units and 6.4×10^2 CEMA units. When annealed at 105 ± 2 °C, P*t*BA is distributed as approximately hexagonally packed cylinders in the PCEMA matrix. Films, 0.05−2.0 μm thick, consisting of this organized array of two incompatible phases, were obtained from microtomy. They were processed, as shown in Scheme 1 in two steps: (I) photo-cross-linking of the PCEMA matrix and (II) hydrolysis of the *tert*-butyl ester groups. First presented below is spectroscopic evidence showing the occurrence of the above reactions.

Photochemical Cross-Linking of the PCEMA Phase. The photochemical reaction involves a 2 + 2 cycloaddition of two double bonds.[22,23] This can occur either between alkenes attached to the same chain or between alkenes linked to two different chains. Only the latter process results in the desired "locking-in" of the PCEMA matrix. Due to the high degree of PCEMA interchain mixing, we anticipated that interpolymeric cycloaddition would be quite effective, as observed in our previous studies.[24−29] The extent of PCEMA double-bond conversion was monitored by UV spectroscopy, following the absorbance decrease at 274 nm upon irradiation. This measurement could not be performed directly on the microtomed films, due to their small size, with respect to the diameter of the spectrometer beam. Instead, spin-

(17) Tanaka, H.; Hasegawa, H.; Hashimoto, T. *Macromolecules* **1991**, *24*, 240.
(18) Sakurai, S.; Hashimoto, T.; Fetters, L. J. *Macromolecules* **1996**, *29*, 740.
(19) *Reagent Chemicals, American Chemical Society Specifications*, 6th ed.; American Chemical Society: Washington, DC, 1981; pp 25−26.
(20) Lide, D. R. *Handbook of Chemistry and Physics*, 76th ed.; CRC Press: Boca Raton, 1995.
(21) Van Krevelen, D. W. *Properties of Polymers*, 3rd ed.; Elsevier Science Publishers: Amsterdam, 1990.
(22) Kato, M.; Ichijo, T.; Ishii, K.; Hasegawa, M. *J. Polym. Sci., Part A: Polym. Chem.* **1971**, *9*, 2109.
(23) Guillet, J. E. *Polymer Photophysics and Photochemsitry − An Introduction to the Study of Photoprocesses in Macromolecules*; Cambridge University Press: Cambridge, UK, 1985.
(24) Guo, A.; Tao, J.; Liu, G. *Macromolecules* **1996**, *29*, 2487.
(25) Tao, J.; Liu, G.; Ding, J.; Yang, M. *Macromolecules* **1997**, *30*, 4084.
(26) Tao, J.; Stewart, S.; Liu, G.; Yang, M. *Macromolecules* **1997**, *30*, 2738.
(27) Ding, J.; Liu, G. *J. Phys. Chem. B* **1998**, *102*, 6107.
(28) Ding, J.; Liu, G. *Chem. Mater.* **1998**, *10*, 537.
(29) Liu, G.; Qiao, L.; Guo, A. *Macromolecules* **1996**, *29*, 5508.

Scheme 2. Hydrolysis of *tert*-Butyl Groups

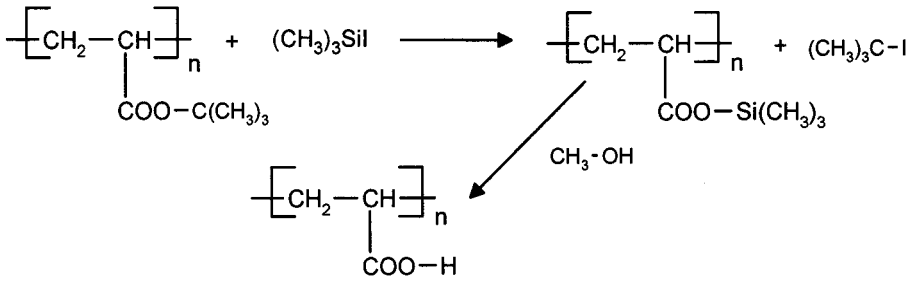

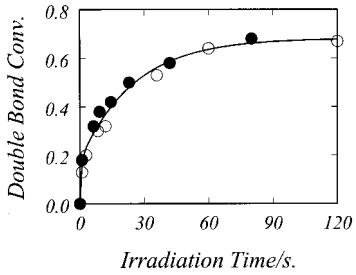

Figure 1. Plot of PCEMA double-bond conversion as a function of UV irradiation for spin cast films which are 28 (○) and 30 (•) nm thick.

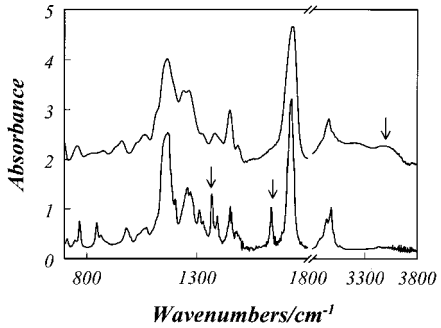

Figure 2. Comparison of FTIR absorption spectra of cross-linked 50-μm-thick PI-*b*-P*t*BA-*b*-PCEMA films before (bottom) and after (top) treatment with $(CH_3)_3SiI$ and methanol.

cast films of various thickness were employed for this study. The kinetics of double-bond conversion in the films is shown in Figure 1 in the case of 28-nm- and 30-nm-thick films. The data were used to approximate the kinetics of the reaction in microtomed films of similar thickness. Typically, the CEMA conversion was controlled at ~40% for the microtomed films.

Hydrolysis of the tert-Butyl Groups. The hydrolysis was carried out in two steps, as depicted in Scheme 2. The irradiated films were treated with trimethylsilyl iodide, to effect the conversion of the *tert*-butyl groups into trimethylsilyl groups.[30] The trimethylsilyl groups then readily hydrolyze in either water or methanol. To ascertain that the reactions take place in polymer films as they do in solution, we carried out a series of FTIR experiments using 50-μm films of a related copolymer, PI-*b*-PCEMA-*b*-P*t*BA. This sample consists of 3.7×10^2 isoprene units, 4.2×10^2 CEMA units and 5.5×10^2 *t*BA units. In the bulk, the P*t*BA block exists as interconnected cylinders, as is discussed elsewhere.[31] Films of this triblock were irradiated and soaked in a trimethylsilyl iodide solution in methylene chloride for 2 weeks. Illustrated in Figure 2 is the comparison between the FTIR spectra of the sample before and after the hydrolysis step. The disappearance of the peak at 1366 cm^{-1} upon the treatment suggests the almost quantitative removal of the *tert*-butyl groups. Since the microtomed P*t*BA-*b*-PCEMA films used in this study are much thinner, it can be reasonably assumed that the quantitative removal of the *tert*-butyl groups took place in this case as well upon treatment with trimethylsilyl iodide and methanol. Unfortunately, the FTIR method was not sensitive enough to allow us to monitor the reactions in the microtomed films directly. However, silicon-specific imaging experiments as will be described later demonstrated the occurrence of the reactions in such thin films.

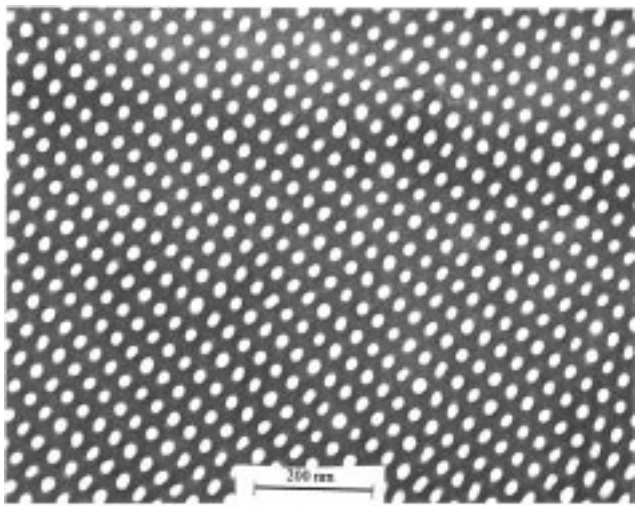

Figure 3. TEM image of a small area of a 50-nm-thick P*t*BA-*b*-PCEMA film annealed at 105 ± 2 °C. The sample was stained with OsO_4.

Film Morphologies. TEM and sometimes SAXS analyses were performed on samples at each stage of the process shown in Scheme 1 to establish the morphology of the films and to assess how the chemical transformations affect the size and shape of the microdomains.

Films of PtBA-b-PCEMA. All samples used in the study were prepared from a solid sample of the block copolymer annealed at 105 ± 2 °C for 21 days. A micrograph of a microtomed section of this sample, stained with osmium tetraoxide prior to viewing, is shown in Figure 3. Since OsO_4 selectively reacts with the double bonds of PCEMA, the light circles correspond to P*t*BA cylinders, of radius $R = 11 \pm 2$ nm, pointing normal to the plane of the image.

Due to the small area imaged in Figure 3, all cylinders appear highly ordered and well aligned. In reality, the

(30) Jung, M. E. Lyster, M. A. *J. Am. Chem. Soc.* **1976**, *99*, 968.
(31) Ding, J.; Stewart, S.; Liu, G. *Angew. Chem., Int.* **1999**, *38*, 835.

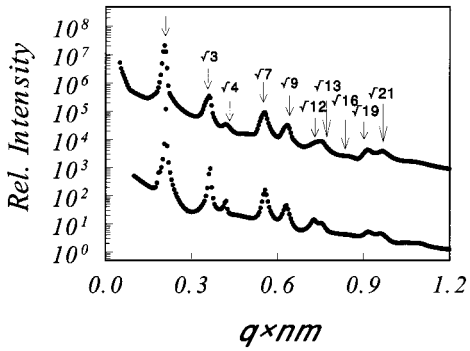

Figure 4. Plot of relative intensity of scattered X-ray as a function of wave vector, q. The bottom curve is the best fit to the experimental data (top) from a paracrystal model.

cylinder orientation changes from grain to grain, which is of the size of micrometers. This is reasonable, because no special measure, such as mechanically shearing[32] or electrically poling[33] the sample, was taken to align the cylinders macroscopically.

A hexagonal array of cylinders was anticipated for this sample, on the basis of the composition of the diblock copolymer. It is interesting to note that the array of cylinders does not exhibit the expected hexagonal symmetry. Instead, the cylinders are aligned with the closest neighbor distances, D_L and D_S, of 44 and 35 nm along the long and short axes, respectively. The angle between short and long axes is ~75°. This nonhexagonal packing is probably due to shear-induced deformation of the matrix during microtoming. Nonetheless, we can use the R, D_L, and D_S values and the angle between the two axes to calculate the volume fraction of the P*t*BA block, which is $\pi R^2/(D_L D_S \sin 75)$ or 0.26. This value is identical within experimental error to that evaluated from the mass fraction of the two blocks.[30]

SAXS results also confirmed the presence of an ordered phase in samples annealed at 105 °C, with the primary scattering peak q_{100} at 0.213 nm^{-1} (Figure 4). The positions of the higher order peaks close to $\sqrt{3}q_{100}$, $\sqrt{4}q_{100}$, $\sqrt{7}q_{100}$, ..., and $\sqrt{27}q_{100}$ suggest that the cylinders are packed with approximate hexagonal symmetry. This indicates that the nonhexagonal cylinder packing observed by TEM may have indeed resulted from matrix deformation during sample microtoming. Furthermore the occurrence of several higher order peaks suggests that the cylinders have long-range ordering. The sharpness of the peaks suggests a narrow distribution of intercylinder distances. A more quantitative description of the cylindrical morphology was obtained by analyzing the experimental SAXS profile (Figure 4) using an equation derived from a paracrystal model.[34,35] This model assumes that (1) the aspect ratio of the cylinders is large, (2) the cylinders are packed parallel to each other with hexagonal symmetry in micrometer-sized grains, (3) the orientation of the grains is random, and (4) the interface between the P*t*BA and PCEMA domains is sharp. Parameters used in the curve fitting

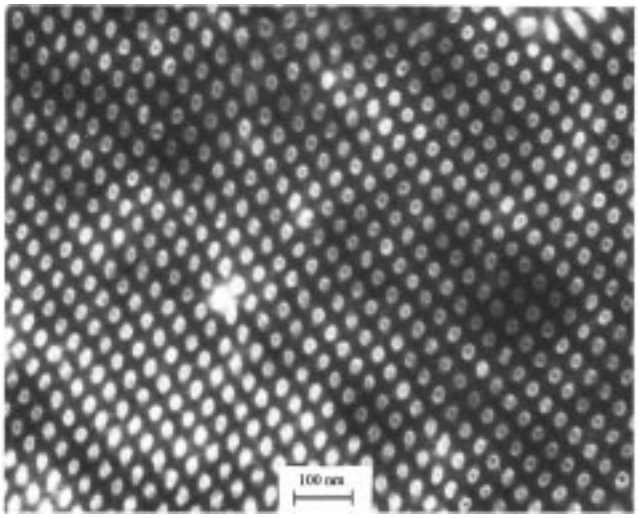

Figure 5. Silicon-specific TEM image of a small area of a 50-nm-thick PtBA-*b*-PCEMA film after reaction with $(CH_3)_3SiI$. This sample was not stained.

equation are the mean closest neighbor distance D (34 nm), with a standard deviation ΔD (1 nm) and the mean radius of the cylinders R (8.5 nm) with a standard deviation ΔR (1 nm). From $(2\pi\sqrt{3})(R/D)^2$, the volume fraction of the P*t*BA domain was determined as 0.23, a value slightly lower than the volume fraction (0.26) obtained from TEM and mass fraction calculations. The difference may be attributed to a relatively wide distribution in R ($\Delta R = 1$ nm).

Cross-Linked Films. Cross-linked films treated with trimethylsilyl iodide (step 1, Scheme 2) were observed by TEM using electrons with an energy of (10^5−110) eV. A micrograph of a small area of the silylated film is shown in Figure 5. Cylinders with a radius of 11 nm appear as bright objects, revealing the presence of silicon (binding energy of the L-shell electrons of Si: ~110 eV).[36] Films treated subsequently with methanol/water could not be imagined under these conditions to obtain good contrast, revealing conversion of the trimethylsilyl groups to acrylic acid. The methanol-treated films were imaged under normal conditions (Figure 6) without staining. The contrast between the cylinders and the continuous phase is attributed to a difference in density between the two regions. We note, in Figure 6, that the projection of some of the nanochannels is not perfectly circular, but slightly elliptic. This may indeed be the true shape of the nanochannels, or else, it may reflect the fact that the cylinders are not perfectly perpendicular to the plane of the image.[29] The radius of the cylinders, obtained from the short axis of the ellipses in Figure 7, is 6 ± 1 nm. This is significantly smaller than the radius of the cylinders, 11 ± 2 nm, measured in the native (Figure 3) and silylated films (Figure 5).

This small cylindrical domain size can be well explained by assuming that the light domains of Figure 6 are void. The void channels form due to the collapsing of the dry PAA chains onto the PCEMA walls. The void channel radius is less than 11 ± 2 nm because only 44% of the polymer weight is lost upon *tert*-butyl removal

(32) See, for example: Winter, H. H.; Scott, D. B.; Gronski, W.; Okamoto, S.; Hashimoto, T. *Macromolecules* **1993**, *26*, 7236.
(33) See, for example: Morkved, T. L.; Lu, M.; Urbas, A. M.; Ehrichs, E. E.; Jaeger, H.; Mansky, P.; Russell, T. P. *Science* **1996**, *273*, 931.
(34) Hashimoto, T.; Kawamura, T.; Harada, M.; Tanaka, H. *Macromolecules* **1994**, *27*, 3063.
(35) Shibayama, M.; Hashimoto, T. *Macromolecules* **1986**, *19*, 740.
(36) Ahn, C. C.; Krivanek, O. L.; Burgner, R. P.; Disko, M. M.; Swann, P. R. *EELS Atlas*; Gatan Inc.: Warrendale, PA, 1983.

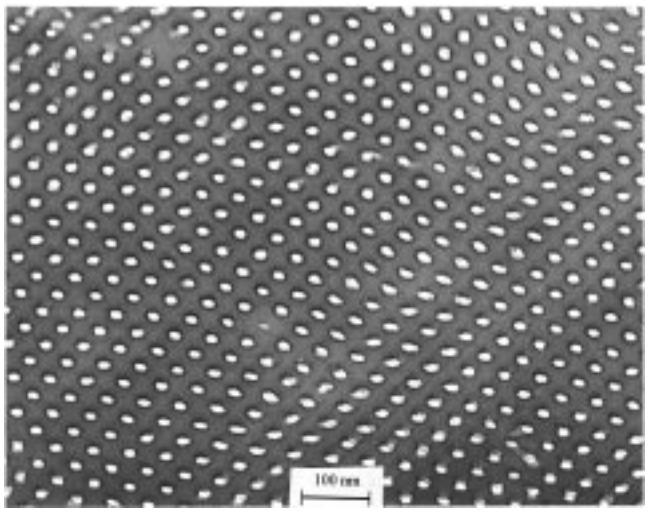

Figure 6. TEM image of a small area of a 50-nm-thick PCEMA-*b*-PAA film. The film was not stained.

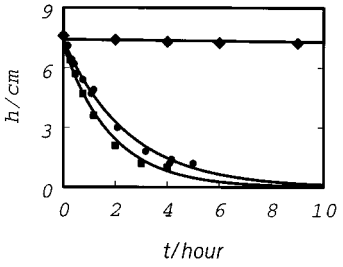

Figure 7. Variation in the water height difference *h* between the two arms of a U-tube as a function of time *t*. The water transport rate is the slowest at pH = 3.0 (◆) but increased at pH = 1.0 (•) and pH = 13.0 (■).

from P*t*BA. Assuming that the densities of P*t*BA and the dry PAA chains are the same, the radius of the void cylinders should be $r = \sqrt{0.44}R$. Using $R = 11 \pm 2$ nm, we find $r = 7 \pm 2$ nm, in agreement with the short axis of the ellipses observed in Figure 6.

Permeability of Films with Poly(acrylic acid)-Lined Nanochannels. The permeability of the PAA-lined membranes was assessed by a simple test using a U-tube filled to different heights with water, as described in the Experimental Section. Water flows from one arm of the tube to the other, due to the difference in height *h* between the liquid columns in the two arms of the tube. The value of *h* was monitored as a function of time for tubes filled with aqueous solutions at different pH and the results obtained at pH 1, 3, and 10 are shown in Figure 7. Also shown are the best fits (solid lines) of the experimental data by eq 4. From these fits, the λ values are obtained and plotted in Figure 8 as a function of pH. The water permeability is high at low and high pH but decreases by more than 2 orders of magnitude at pH 3.

These initial results demonstrate the great potential of the nanochannel membranes to act as "chemical valves". Chemical valve effects are also exhibited by currently available filtration membranes, such as nuclear track-etched membranes with a diameter of ~0.20 μm and grafted with PAA or poly(*L*-glutamic acid).[16,37−39]

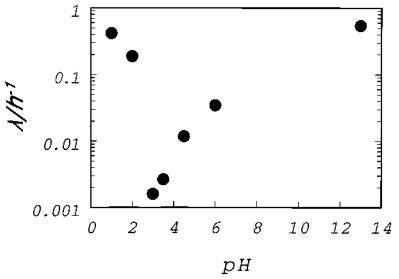

Figure 8. Variation in membrane permeability constant, λ, as a function pH.

The water permeability of these membranes decreases smoothly with increasing pH. The water permeability is high at low pH because the PAA chains are collapsed at low pH, leaving the pores wide open. At high pH, the ionized PAA chains are outstretched and block the pores to a significant extent, reducing the flow of water.

The permeability behavior of the membranes described here are different, and the difference can be attributed to the high graft density and to the fact that the channels are small compared to the length of the PAA chains. We estimate that the length of the fully stretched PAA chains is ~95 nm. Individual chains can fold several times across a channel of the diameter of 22 nm. Although the nanochannels in Figure 6 seem void when dry, the chain segments in water should be distributed uniformly inside the nanochannels, regardless of the pH. A simple geometric analysis, using a channel radius value of 11 nm, reveals that the density of PAA chains on the PCEMA walls is $\sim 7 \times 10^{12}$ chains/cm^2, a value substantially higher than the grafting densities attainable by conventional techniques, such as diblock adsorption in a block-selective solvent,[40−43] and, probably, than the graft density of the nuclear track-etched membranes.[16]

The water permeability variation pattern observed here may reflect how the PAA chain segmental mobility changes with pH. At pH = 3, the AA units are neutral, the PAA chains take up little water, and the neutral AA units form a "cross-linked" gel inside a nanochannel due to hydrogen bonding.[16] The "cross-linking" may reduce both the amplitude and the frequency of wriggling motions of the chains. The reduced motion of the chain segments means the reduced rate at which the segments make space for the water molecules to hop or diffuse through the channels and water permeation rate is thus the lowest at this pH. As pH decreased, the hydrogen bonds were probably broken by protons, which increased the chain segment mobility and thus water permeability. Water permeability increased at high pH, as AA groups were converted into sodium acrylate, which did not form hydrogen bonds. Also, ionized carboxyl groups took up more water for solvation.

(37) Ito, Y.; Ochiai, Y.; Park, Y. S.; Imanishi, Y. *J. Am. Chem. Soc.* **1997**, *119*, 1619.

(38) Ito, Y.; Kotera, S.; Inaba, M.; Kono, K.; Imanishi, Y. *Polymer* **1990**, *31*, 2157.

(39) Winnik, F. M.; Morneau, A.; Mika, A. M.; Childs, R. F.; Roig, A.; Molins, E.; Ziolo, R. F. *Can. J. Chem.* **1998**, *76*, 10.

(40) Tao, J.; Guo, A.; Liu, G. *Macromolecules* **1996**, *29*, 1618.

(41) Ding, J.; Birss, V. I.; Liu, G. *Macromolecules* **1997**, *30*, 1442.

(42) Ding, J.; Tao, J.; Guo, A.; Stewart, S.; Hu, N.; Birss, V. I.; Liu, G. *Macromolecules* **1996**, *29*, 5398.

(43) Tao, J.; Guo, A.; Stewart, S.; Birss, V. I.; Liu, G. *Macromolecules* **1998**, *31*, 172.

As defined in eq 5, the λ parameter of Figure 8 is equal to $2PA\rho g/\sigma l$, where A is the total permeable nanochannel cross-section, P the pressure drop across the two arms of the U-tube, ρ the water density, g the gravitational acceleration constant, σ the cross-section of the U-tube, and l the thickness of the membrane. Since we do not know the value of A, it is difficult to determine the nanochannel permeability constant, P. As a first approximation, we assume that all the channels are perpendicular to the membrane surface and that they span the entire film. Since the nanochannels occupy ~26% of the membrane surface area (~1 mm^2), the permeable cross-section A should be ~0.26 mm^2. With this value for A and $\rho = 1.0$ g cm^{-3}, $g = 980$ cm s^{-2}, $l = 2.0 \times 10^{-4}$ cm, $\lambda = 0.42$ h^{-1}, we calculated $P = 0.92 \times 10^{-8}$ cm^2 Pa^{-1} s^{-1} at pH = 1. This nanochannel permeability compares well with the values reported for the PAA grafted nuclear track-etched membranes. Moreover, since not all the channels span the whole film thickness or some channels lie parallel to the membrane surface as revealed by TEM, the estimated value of P should be regarded as a lower limit.

We also carried out permeability measurements for aqueous solutions of various ionic strengths and containing divalent cations. For example, at pH 6.0, λ takes values of 0.034 and 0.097 h^{-1} for pure water and aqueous 0.10 M NaCl, respectively. This result is easily understood, if one recalls that at pH 6 the PAA chains are partially ionized and that the addition of salt has a screening effect, leading to more chain flexibility in the channels.

The membranes exhibited a striking sensitivity to the presence of divalent cations. An aqueous 1.0 M calcium chloride solution did not permeate through the membrane, as evidenced by the fact that the difference in height h in the U-tube testing device remained constant for 28 h. The nanochannels appeared to be completely blocked, probably as a result of the formation of a network of PAA chains cross-linked by ionic interactions with Ca^{2+}.[44] This striking result suggests that the membranes may act as sensors or valves.

Membranes as Hosts for Inorganic Particles. To explore the possible use of the novel membranes as templates for the preparation of nanoparticles, we modified the membranes by impregnating them with either a semiconductive materiel, CdS, or a magnetic material, Fe_2O_3. To introduce CdS, the films were soaked in a cadmium acetate solution and subsequently exposed to hydrogen sulfide. The modified films were studied by TEM. A side view of the nanochannels partially filled with CdS is presented in Figure 9a. Discreet particles are found throughout the straight and long channels. No long inorganic cylinders were detected in the sample. An end view of the nanochannels is shown in Figure 9b. Some of the CdS nanoparticles have a light core, suggesting that they may be hollow. The electron diffraction pattern obtained for the CdS particles presents seven visible halos (Figure 10). The interplane distances, d_{hkl}, are listed in Table 2, together with literature values. The agreement between our d_{hkl} values and the literature values is excellent. We also compared the relative intensities of the different halos to those reported, and these comparisons suggest that the particles formed are β-CdS crystals with a cubic zinc blende structure.[45,46]

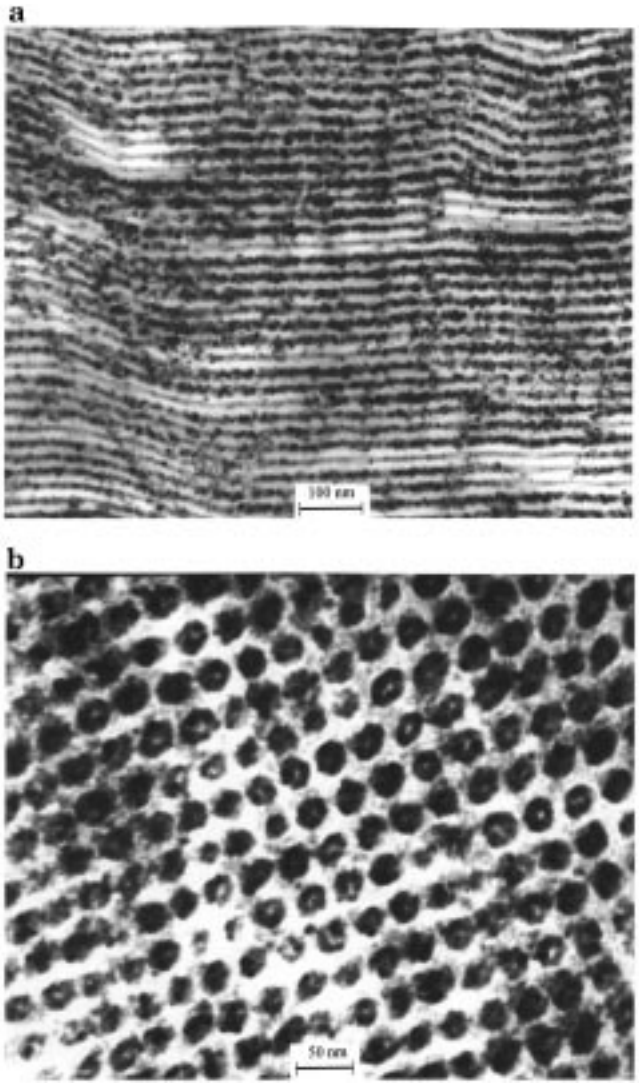

Figure 9. PAA nanochannels filled with CdS particles: (a) side and (b) end-on view.

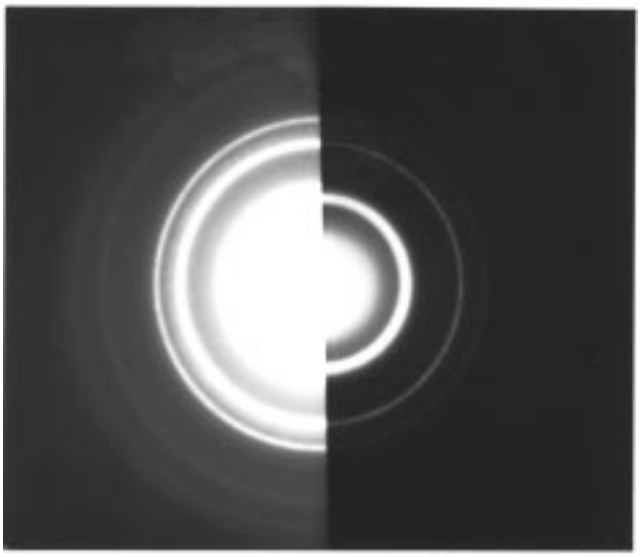

Figure 10. Electron-diffraction pattern of the CdS particles. Lighter and larger halos are seen only in the more exposed half.

(44) Wall, F. T.; Drenan, J. W. *J. Polym. Sci.* **1951**, *7*, 83.

Table 2. Interplanar Spacings of CdS and Fe_2O_3 Particles and Their Comparison with Literature Values

d_{hkl}, Å (exptl)	d_{hkl}, Å	Miller Indices: *hkl*
	CdS	
3.36	3.36	111
2.06	2.06	220
1.75	1.75	311
1.33	1.33	331
1.19	1.19	422
1.11	1.12	333, 511
0.98	0.98	531
	Fe_2O_3	
2.49	2.51	311
2.15	2.09	400
1.61	1.60	511, 333
1.46	1.47	440

Magnetic membranes were obtained by in situ precipitation of iron oxide into films impregnated with a ferrous chloride solution following a procedure used previously to prepare magnetic PAA-grafted polypropylene membranes.[39] The Fe^{2+}-loaded membranes were thoroughly washed in water, and then immersed in aqueous sodium hydroxide solution and treated with oxygen. A micrograph of an end view of the resulting membrane shows iron oxide nanoclusters, ~10 nm in diameter, located exclusively in the nanochannels. No nanowires formed under these conditions. From the electron diffraction pattern obtained from the iron oxide particles we determined that they consisted of γ-Fe_2O_3 (see Table 2).[47] The membranes were attracted by a small magnet. Unfortunately we were unable to measure their magnetic properties by SQUID magnetometry, which did not have adequate sensitivity to detect the magnetization of the small membranes available (<1 cm^2).

There exist various methods for the production of semiconductor and magentic nanoparticles. Magnetic nanoparticles have, for example, been produced in polymer films,[48] in polymer gel particles,[49] in microemulsion droplets,[50] in lipid vesicles,[51] or in water or oil under controlled formation conditions.[52] Similar methods can be used for the production of semiconductor nanoclusters[53] or nanowires.[54] Magnetic nanoparticles are of interest mainly for their superparamagnetism.[55] They can, for example, be used in immonoassay,[56] water reclamation,[57] or the probing of the local viscoelasticity of living cells.[58] Semiconductor nanoparticles have been of interest mainly for their quantum size effect. The apparent advantage of our method for nanoparticle preparation is that the inorganic particle size is controlled by that of the nanochannels.

VI. Conclusion

A P*t*BA-*b*-PCEMA sample was synthesized and characterized. After annealing at 105 °C, the P*t*BA block formed densely packed cylinders inside the PCEMA matrix, as confirmed by TEM and SAXS results. Thin films of the diblock were obtained by microtomy. After PCEMA cross-linking by UV irradiation, the *tert*-butyl groups of P*t*BA were hydrolyzed, leaving PAA chains in the nanometer-sized cylinders. Thin films with such loosely packed cylinders functioned as membranes. The permeability of water across such membranes varied sharply depending on the pH and the ionic strength of the aqueous medium and the cation valence in it. Such membranes may find applications as chemical sensors or chemical valves. The membranes were also used as template for the preparation of CdS and γ-Fe_2O_3 nanoparticles.

Acknowledgment. NSERC of Canada is cordially acknowledged for the financial support of this research. Dr. A. Guo is thanked for preparing the diblock used.

CM990184K

(45) Traill, R. J.; Boyle, R. W. *Am. Mineral.* **1955**, *40*, 555.
(46) Routkevitch, D.; Bigioni, T.; Moskovits, M.; Xu, J. M. *J. Phys. Chem.* **1996**, *100*, 14037.
(47) Joint Committee on Powder Diffraction. *Mineral Powder Diffraction File Data Book*; International Center for Diffraction Data: Pennsylvania, 1980; Vol. 1.
(48) (a) Ziolo, R. F.; Giannelis, E. P.; Weinstein, B. A.; O'Horo, M. P.; Ganguly, B. N.; Mehrotra, V.; Russell, M. W.; Huffman, D. R. *Science* **1992**, *257*, 219. (b) Winnik, F. M.; Morneau, A.; Mika, A. M.; Childs, R. F.; Roig, A.; Molins, E.; Ziolo, R. F. *Can. J. Chem.* **1998**, *76*, 10. (c) Yamaguchi, K.; Sato, T.; Kato, Y.; Inoue, M.; Fujii, T. *Mater. Sci. Forum* **1998**, *287*−*288*, 483. (d) Sohn, B. H.; Cohen, R. E. *Chem. Mater.* **1997**, *9*, 264. (e) Jarjayes, Fries, P. H.; Bidan, G. *J. Magnet. Magnet. Mater.* **1994**, *137*, 205.
(49) (a) Winnik, F. M.; Morneau, A.; Ziolo, R. F.; Stover, H. D.; Li, W. H. *Langmuir* **1995**, *11*, 3660. (b) Kroll, E.; Winnik, F. M.; Ziolo, R. F. *Chem. Mater.* **1996**, *8*, 1594.
(50) (a) Lopez-Quintela, M. A.; Rivas, J. *Curr. Opin. Colloid Interface Sci.* **1996**, *1*, 806. (b) Lopez-Perez, J. A.; Lopez-Quintela, M. A.; Mira, J.; Rivas, J.; Charles, S. W. *Phys. Chem. B.* **1997**, *101*, 8045.
(51) (a) Mann, S. Skarnulis, J.; William, R. J. P. *J. Chem. Soc., Chem. Commun.* **1979**, 1030. (b) Yaaco, I. I.; Nunes, A. C.; Bose, A. *J. Colloid Interface Sci.* **1995**, *171*, 73.
(52) (a) Lefebure, S.; Dubois, E.; Cabuil, V.; Neveu, S.; Massart, R. *J. Mater. Res.* **1998**, *13*, 2975. (b) Matijevic, E. *Prog. Colloid Polym. Sci.* **1996**, *101*, 38.
(53) (a) Kane, R. S.; Cohen, R. E.; Silbey, R. *Chem. Mater.* **1999**, *11*, 90. (b) Lippens, P. E.; Lannoo, M. *Phys. Rev. B.* **1990**, *41*, 6079. (c) Eychmuller, A.; Katsikas, L.; Weller, H. *Langmuir* **1990**, *6*, 1605. (d) Bawendi, M. G.; Kortan, A. R.; Steigerwald, M. L.; Brus, L. E. *J. Chem. Phys.* **1989**, *91*, 7282.
(54) Morales, A. M.; Lieber, C. M. *Science* **1998**, *279*, 208.
(55) Leslie-Pelecky, D. L.; Rieke, R. D. *Chem. Mater.* **1996**, *8*, 1770.
(56) (a) Sutor, J. J. USA Patent 5,648,124, 1997. (b) Muller-Schelte, D.; Brunner, H. *J. Chromatogr. A* **1995**, *711*, 53. (c) Li, X.; Sun, Z. *J. Appl. Polym Sci.* **1995**, *58*, 1991. (d) Kondo, A.; Fukuda, H. *J. Ferment. Bioengin.* **1997**, *84*, 337.
(57) Kolaris, L. O.; Anderson, N. J.; Bolto, B. A.; Chin, C. T.; Priestley, A. J. *Water Supply* **1994**, *13*, 253.
(58) Bausch, A. R.; Moller, W.; Sackmann, E. *Biophys. J.* **1999**, *76*, 573.